Upper critical field and the Fulde-Ferrel-Larkin-Ovchinnikov transition in multiband superconductors

A. Gurevich

National High Magnetic Field Laboratory, Florida State University, Tallahassee, Florida 32310, USA

The effect of orbital and Zeeman pair breaking on the upper critical field H_{c2} and the Fulde-Ferrel-Larkin-Ovchinnikov (FFLO) transition in clean anisotropic multiband superconductors is addressed. For a uniaxial superconductor with a single parabolic band, a close form equation for $H_{c2}(T, \theta)$ as functions of temperature T and the angle θ between **H** and the c axis is obtained. The wave vector **Q** of the FFLO oscillations is shown to be not parallel to the magnetic field **H** if it is tilted away from the symmetry axis. For multiband superconductors, the crystalline anisotropy, and the $s^{\pm}$ pairing symmetry with the sign change of the order parameter on different sheets of the Fermi surface can significantly increase the orbitally limited H_{c2} and facilitate the FFLO transition. It is shown that if shadow bands exist close to the Fermi level (as characteristic of ferropnictides), a small shift of the chemical potential upon doping can trigger the FFLO transition produced by emerging small pockets of the Fermi surface even for moderate values of the Maki parameter in the main bands.

I. INTRODUCTION

The discovery of superconductivity in the diverse family of ferropnictides[1] has renewed interest in multiband superconductivity caused by *strong interband* pairing mediated by antiferromagnetic excitations.[2–5] In this respect pnictides are different from the classic two-band superconductor MgB$_2$ in which the critical temperature $T_c = 40$ K, although not significantly lower than the maximum $T_c \simeq 55$ K for oxypnictides, results from strong intraband electron-phonon interaction and *weak interband coupling*.[6–8] Besides their high T_c oxipnictides exhibit very high upper critical fields $H_{c2}(T)$, which often extrapolate to $H_{c2}(0) \sim 100$–200 T because of extremely high slopes $dH_{c2}/dT \sim 3$–20 T/K at T_c (Refs. 9–20) comparable to only those of heavy-fermions compounds[21–23] and layered organic superconductors.[24,25] High values of $H_{c2} = \phi_0/2\pi\xi^2$ in semimetallic pnictides result from their short coherence lengths $\xi \sim \hbar v/2\pi k_B T_c \sim 1$–$3$ nm due to high T_c and low Fermi velocities $v \sim 10^7$ cm/s.[2–5] Hereafter the common abbreviations of 1111 for ReFeAsO$_{1-x}$F$_x$, 122 for BaFe$_2$As$_2$ and 111 for MFeAs and 11 for FeSe$_{1-x}$Te$_x$ families of ferropnictides will be used (Re is the rare earth element such as La, Sm, and Nd, and M is a metal such as Na, Li, etc.)

At high magnetic fields, 1111 pnictides exhibit convex $H_{c2}(T)$ curves for **H**$\|c$ (Refs. 9 and 10) consistent with the behavior expected from the orbitally limited H_{c2} for multiband pairing[26–29] or multilayered structures.[30,31] At the same time, the concave shape of $H_{c2}(T)$ curves observed on 122, 111, and 11 pnictides show apparent signs of strong Pauli limiting of H_{c2},[10–20] indicating that these materials may be close to the Fulde-Ferrel-Larkin-Ovchinnikov (FFLO) transition[32–36] for which the Zeeman splitting causes a nonzero momentum of the Cooper pairs and oscillations of the superconducting order parameter $\Psi(z)$. Evidences of the FFLO state have been found for heavy fermion[37–40] and organic[41–43] superconductors in which a noticeable low-temperature upturn in $H_{c2}(T)$ indicative of the FFLO state was observed. Manifestations of the FFLO instability for

Bose condensates of cold atoms[44,45] and quark-gluon plasma[46] have also been discussed. Several features of pnictides make them good candidates for the FFLO state: (1) for most pnictides, the observed $H_{c2}(0)$ significantly exceed the BCS paramagnetic limit $H_p[\mathrm{T}] = 1.84 T_c[\mathrm{K}]$ above which the pair-breaking Zeeman energy exceeds the binding energy of the Cooper pair, $H > H_p = \Delta/\mu\sqrt{2}$, where μ is the magnetic moment of a quasiparticle, and Δ is the superconducting gap,[36] (2) many pnictides (particularly 122, 111, and 11 compounds) do exhibit a steep increase of $H_{c2}(T)$ near T_c followed by the flattening of $H_{c2}(T)$ at lower T,[11–20] indicating that the Zeeman pair breaking may dominate over the orbital pairbreaking,[34–36] and $\alpha_M = \sqrt{2}H_{c2}^*/H_p \gtrsim 1$. Here α_M is the Maki parameter[36] in the BCS clean limit

$$\alpha_M = \pi^2 \Delta/2m_0 v^2, \quad \mathbf{H}\|c, \tag{1}$$

$$\alpha_M = \pi^2 \Delta/2m_0 v v_c, \quad \mathbf{H}\perp c \tag{2}$$

where $H_{c2}^* = \phi_0/2\pi\xi^2$ for **H**$\|c$ is calculated without the Zeeman pair breaking, $\xi = \hbar v/\pi\Delta$, v and v_c are the Fermi velocities in the ab plane and along the c axis, respectively, m_0 is the free electron mass, and ϕ_0 is the flux quantum. The condition $\alpha_M > 1$ is more easily satisfied in materials with high T_c and low Fermi energy E_F.

For **H**$\|c$, the FFLO instability occurs at $\alpha_M > \alpha_c$, where $\alpha_c \approx 1.8$ for a single-band spherical Fermi surface (FS).[36] In this case the condition $\alpha > \alpha_c$ implies $\Delta \gtrsim E_F$, which cannot happen in a single band electron-phonon superconductor with the effective mass $m \sim m_0$. The criterion $\alpha_M > \alpha_c$ can be satisfied more easily in strongly anisotropic materials (such as organic superconductors) in a magnetic field parallel to the layers in which case α_M is enhanced by the large v/v_c ratio. It is the FFLO state for **H**$\|ab$, which has been mostly investigated in the literature.[47–49] The FFLO instability is also facilitated in heavy-fermion superconductors,[21–23] where the huge band mass $m \gg m_0$ and low Fermi velocity make it possible to satisfy both conditions $\alpha_M \gtrsim 1$ and $\Delta \ll E_F$. Nonmagnetic impurities increase H_{c2}^* thus enhancing the Zeeman

pair breaking but suppressing the FFLO instability,[35,50] the situation can be more complicated for the d-wave pairing.[51] For the optimally doped Nd-1111 with $v = 1.3 \times 10^7$ cm/s (Refs. 52–54) and $T_c = 55$ K, Eq. (1) gives the Maki parameter $\alpha_M \simeq 0.4$ which can increase in the underdoped state as one of the Fermi velocities decreases and m increases. However, as shown below, such single-band estimates can underestimate the FFLO instability criterion in $s^{\pm}$ superconductors.

The concave shapes of $H_{c2}(T)$ observed on 122 and 11 compounds are indicative of strong Pauli limiting both for $\mathbf{H} \| c$ and $\mathbf{H} \| ab$ with a moderate mass anisotropy $m_c \lesssim (3-10)m$ but only weakly anisotropic H_{c2}.[10–20] At the same time, the band effective masses $m \simeq (2-5)m_0$ although enhanced by the interaction with magnetic modes,[2–5] are still much smaller than those in heavy-fermion compounds. This brings about the question to what extent the observed signs of the Pauli limiting in $H_{c2}(T)$ of pnictides could result from multiband effects and unconventional pairing symmetry, and how would they affect the FFLO transition for bands with different anisotropy, superconducting gaps, Fermi energies, densities of states, etc. Particularly, if the conditions $\alpha_M > \alpha_c$ calculated from Eqs. (1) and (2) are satisfied only for one band, can a global FFLO transition still occur?

In multiband superconductors the orbital pair breaking and the FFLO instability can be tuned by doping. For example, for disconnected electron and hole FS sheets (such as in MgB$_2$ and pnictides), the shift of the chemical potential expands one FS and shrinks the other. Since $\alpha_M \propto 1/E_F$ increases for the shrinking FS and decreases for the expanding FS, the shrinking FS pocket can reach the FFLO instability while the expanding FS moves away from it. This poses the question if the shrinking FS may enforce the global FFLO state. Moreover, in pnictides several shadow bands happen to be only slightly below the Fermi level (for example, the hole band at the Γ point in 122 and 11 compounds), resulting in changes in superconducting properties and even the pairing symmetry upon a small shift of the chemical potential.[52–54] In this case a small FS pocket emerging upon doping (similar to the Lifshitz transition) would have a large $\alpha_M \propto 1/E_F$ while not significantly affecting global superconducting properties controlled by the main electron and hole pockets in Γ and M points in the Brillouin zone. Then the issue whether a small FS pocket with $\alpha_M > \alpha_c$ could trigger the FFLO transition if the main bands have $\alpha_M < \alpha_c$ is to be addressed.

In this paper the role of multiband effects, electronic anisotropy, pairing symmetry, and Zeeman pair breaking on $H_{c2}(T)$ and the FFLO instability are addressed. It is shown that the $s^{\pm}$ pairing in the case of strong anisotropy of one of the FS sheets can increase the orbitally limited H_{c2}^* and facilitate the FFLO transition as compared to the more conventional s^{++} pairing in MgB$_2$. The solution of the linearized gap equations gives the variety of different behaviors for $H_{c2}(T)$, for example, the Sarma-type $H_{c2}(T)$ curves for paramagnetic pair breaking at $\alpha_M \gg 1$,[36] or $H_{c2}(T)$ with upward curvature, or $H_{c2}(T)$ curves similar to those of the conventional Werthamer-Helfand-Hohenberg (WHH) theory.[35] However, unlike single-band superconductors for which the Zeeman pair breaking becomes apparent as the shape of $H_{c2}(T)$

changes at large α_M, the case of multiband superconductors can be more subtle. In particular, the FFLO transition for the $s^{\pm}$ pairing can occur even if one band has $\alpha_M < \alpha_c$ and the temperature dependence of $H_{c2}(T)$ exhibits no apparent features of strong Pauli pair breaking characteristic of a single-band superconductor. The paper is organized as follows.

In Sec. II a single-band uniaxial superconductor is considered. Using the WHH approach, an exact solution for $\Psi(\mathbf{r})$ and the equation for $H_{c2}(T, \theta)$, which take into account both orbital and paramagnetic pair-breaking effects at arbitrary orientation of $\mathbf{H}$, is given. It is shown that for $\mathbf{H}$ inclined by the angle θ with respect to the c axis, the FFLO vector $\mathbf{Q}$ is not parallel to $\mathbf{H}$ except for $\mathbf{H}$ directed along the c axis or ab planes.

In Sec. III $H_{c2}(T)$ and the FFLO transition in multiband superconductors at $\mathbf{H} \| c$ are considered. The orbitally limited $H_{c2}(T)$ curves for $\alpha_M \ll 1$ exhibit distinct upward curvatures but rather different behaviors for the $s^{\pm}$ and s^{++} pairing symmetries. The $s^{\pm}$ pairing can significantly enhance H_{c2} and facilitate the FFLO transition as compared to the s^{++} case. A mechanism of the FFLO transition triggered by opening up a new FS pocket is proposed.

Section IV contains the discussion of the results, particularly in light of recent high field H_{c2} measurements on ferropnictides. Implications of the FFLO state on the vortex structures in anisotropic superconductors and possible experiments to reveal the "hidden" FFLO state are also discussed.

II. ANISOTROPIC SINGLE BAND

In this paper the WHH approach[35] for clean multiband anisotropic superconductors is used. Strong coupling Eliashberg corrections are taken into account by renormalization of the parameters, as shown below. The clean limit seems to be relevant to oxypnictides due to their short in-plane coherence lengths, $\xi_0 \sim 1-2$ nm extracted from H_{c2} measurements on 1111 and 122 single crystals,[10,11] which is also consistent with the observation of quantum oscillations on 1111 and 122 single crystals.[55–58] In this paper we focus on the s-wave singlet pairing and do not consider field-induced triplet components of the order parameter Ψ (Refs. 59–61) or noncentrosymmetric or spin-orbital effects on H_{c2}.[62,63] To fix the notions used later on, we start with a single-band uniaxial superconductor in the uniform field $\mathbf{H}$ inclined by the angle θ with respect to the c axis. In this case the linearized gap equation is given by

$$\Psi(\mathbf{r}) = \int \Psi(\mathbf{r}')d^3\mathbf{r}' \int \frac{d^3\mathbf{k}}{(2\pi)^3} K(\mathbf{k})$$
$$\times \exp\left[i\mathbf{k}(\mathbf{r} - \mathbf{r}') + \frac{i\pi}{\phi_0}\mathbf{H} \cdot (\mathbf{r} \times \mathbf{r}') \right]. \quad (3)$$

The orbital magnetic term in Eq. (3) is represented by the phase factor $\int_{\mathbf{r}'}^{\mathbf{r}} \mathbf{A}d\mathbf{s}$ in the gauge $\mathbf{A} = \frac{1}{2}[\mathbf{H} \times \mathbf{r}]$, and $K(\mathbf{k})$ is the Fourier transform of the Gor'kov kernel. We consider a prolate ellipsoidal FS for a parabolic band with the isotropic in-plane effective mass m and the mass $m_c > m$ along the c
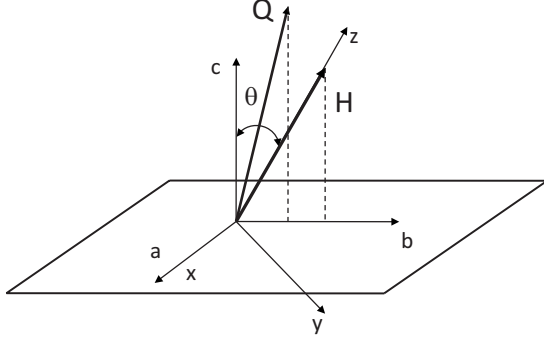
FIG. 1. Coordinate frames used in the calculations: the crystal frame *abc* linked to the symmetry axis of a uniaxial crystal and the field frame *xyz* obtained by rotation of the *abc* frame by the angle θ around the common *a* and *x* axis so that the *z* axis is parallel to **H**. In anisotropic superconductors the FFLO wave vector **Q** is generally not parallel to **H**. We consider here neither the effect of crystal symmetry in the *ab* plane nor anisotropic order parameters (Refs. 47–49 and 64–66) so the orientation of the orthogonal *a* and *b* axes is arbitrary.

axis, for which $K(\mathbf{p})$ is obtained by rescaling the WHH result[35] for the spherical FS

$$K(\mathbf{p}) = \mathrm{Re} \sum_{\omega>0}^{\Omega} \frac{4\pi T\lambda}{v\sqrt{p_\perp^2 + \epsilon p_z^2}} \tan^{-1} \frac{v\sqrt{p_\perp^2 + \epsilon p_z^2}}{2(\omega + i\mu H)}, \quad (4)$$

where $\epsilon = m/m_c = (v_c/v)^2$ is the mass anisotropy parameter, $p_\perp^2 = p_x^2 + p_y^2$, $\omega = \pi T(2n+1)$, $n = 0, \pm 1, \dots, \Omega$ is a cut-off frequency of exchange bosons, μ is the electron magnetic moment, which is assumed independent of the field orientation in a crystal, $\lambda = VN$ is the dimensionless coupling constant, V is the pairing potential averaged over the FS, and $N = m^2 v/2\pi^2\hbar^3\sqrt{\epsilon}$ is the density of states per spin (the units with $k_B = \hbar = 1$ will be used unless stated otherwise). Details of pairing mechanisms are not essential in this model so λ is regarded as a material, field-independent parameter, which can be expressed in terms of T_c. In multiband superconductors the ratios of different elements of the pairing matrix λ_{mn} will be essential (m and n are the band indices). The **p**-momentum frame in Eq. (4) is associated with the *abc* crystal frame shown in Fig. 1.

We choose the **r**-coordinate frame in which $\mathbf{H}\|z$ (see Fig. 1) and seek $\Psi(\mathbf{r})$ in the form

$$\Psi(\mathbf{r}) = \Delta \exp(-c_x h x^2 - c_y h y^2)[C_1 e^{i\mathbf{Qr}} + C_2 e^{-i\mathbf{Qr}}], \quad (5)$$

where $h = \pi H/2\phi_0$, and C_1 and C_2 are complex constants so that $|C_1|^2 + |C_2|^2 = 1$. The Fulde-Ferrel state corresponds to $C_1 = 1$ and $C_2 = 0$ (or $C_1 = 0$ and $C_2 = 1$),[32] and the Larkin-Ovchinnikov state occurs if $C_1 = C_2$.[33] The scaling constants $c_x(\theta)$ and $c_y(\theta)$ and the FFLO wave vector **Q** are determined by the condition that H_{c2} is maximum.

As was shown by WHH,[35] the solution of Eq. (3) is also an eigenfunction of the Schrödinger equation for a particle with a double electron charge in a uniform magnetic field, and of the operator $\hat{W} = i\mathbf{H\Pi}$ where $\mathbf{\Pi} = \nabla + 2\pi i\mathbf{A}/\phi_0$. It turns out that Eq. (5) satisfies both of these conditions. Indeed, $\hat{W}\Psi = -HQ_z\Psi$ in the field frame where $\mathbf{H} = (0,0,H)$ and A_z
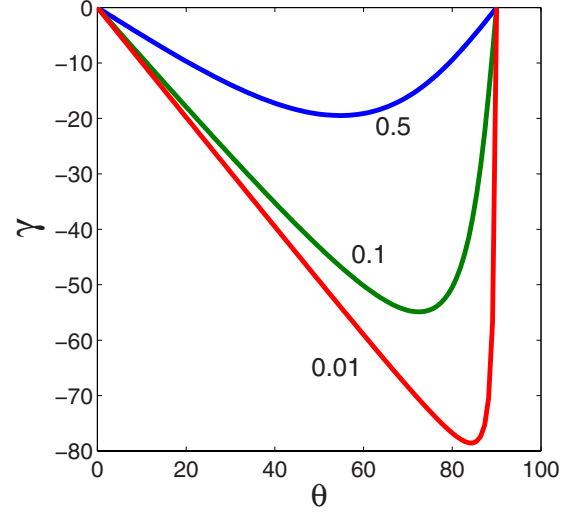
FIG. 2. (Color online) The angle γ between **H** and **Q** defined by Eq. (10) for different values of ϵ.

$= 0$. To show that Eq. (5) is the eigenfunction of the Schrödinger equation, we first write it in the crystal frame

$$\sigma_{\mu\nu}\Pi_\mu\Pi_\nu\Psi = E\Psi, \quad (6)$$

where $\sigma_{\mu\nu} = \mathrm{diag}(1,1,\epsilon)$ is the dimensionless matrix of the electron mass ratios, and $E\hbar^2/2m$ is the particle energy. Next Eq. (6) is transformed into the rotated field frame shown in Fig. 1, where $\sigma_{xx} = 1$, $\sigma_{yy} = \cos^2\theta + \epsilon\sin^2\theta$, $\sigma_{zz} = \sin^2\theta + \epsilon\cos^2\theta$, $\sigma_{yz} = \sigma_{zy} = (1-\epsilon)\sin\theta\cos\theta$, and all other elements of $\sigma_{\mu\nu}$ are zero. Then Eq. (6), which is also the linearized Ginzburg-Landau (GL) equation in which $E = -1$ if all lengths are normalized to $\xi(T)$, becomes

$$[\sigma_{xx}\Pi_x^2 + \sigma_{yy}\Pi_y^2 + \sigma_{zz}\Pi_z^2 + 2\sigma_{yz}\Pi_z\Pi_y]\Psi = E\Psi, \quad (7)$$

where $\Pi_x = \partial_x - 2ihy$, $\Pi_y = \partial_y + 2ihx$, and $\Pi_z = \partial_z$. The function $\Psi(\mathbf{r})$ defined by Eq. (5) satisfies Eq. (7) if: $c_x^2 = \sigma_{yy}$, $c_y^2\sigma_{yy} = 1$ and $Q_x = 0$, $Q_y = -\sigma_{yz}Q_z/\sigma_{yy}$. The first two conditions cancel all terms proportional to x^2, y^2, and xy in Eq. (7) while the second two conditions cancel all terms linear in x and y. This yields the energy of the ground state $E_0 = -4\epsilon_\theta^{1/2}h - \epsilon Q_z^2/\epsilon_\theta$ and

$$c_x = \epsilon_\theta^{1/2}, \quad c_y = \epsilon_\theta^{-1/2}, \quad (8)$$

$$\epsilon_\theta = \cos^2\theta + \epsilon\sin^2\theta. \quad (9)$$

For the field tilted away from the symmetry axis, the FFLO wave vector **Q** is not parallel to **H** but has the transverse component $Q_y = -\sigma_{xy}Q_z/\sigma_{yy}$ projected onto the *ab* plane as shown in Fig. 1 where

$$Q_y = -\frac{Q_z(1-\epsilon)\sin 2\theta}{2(\cos^2\theta + \epsilon\sin^2\theta)}. \quad (10)$$

The angle $\gamma(\theta) = \tan^{-1}(Q_y/Q_z)$ between **H** and **Q** as a function of θ is shown in Fig. 2. Here **Q** is parallel to **H** only if the field is directed along the symmetry axes. For strong anisotropy, $\epsilon \ll 1$, the FFLO oscillations occur mostly along the *c* axis ($Q_y \ll Q_z$) practically for all field orientations except for **H** nearly parallel to the *ab* plane. Here we do not

consider the effect of in-plane crystal symmetry or aniso-tropic pairing, which can result in preferential orientations of $\mathbf{Q}$ in the ab plane for $\mathbf{H} \| ab$.[67] The fact that Eq. (5) is an exact solution of Eq. (6) makes it possible to transform Eqs. (3) and (4) to the isotropic form of the WHH solution for H_{c2} (Ref. 35) by consecutive rotation, rescaling and shift of the momentum frame. The details are given in Appendix A, where it is also shown that H_{c2} is indeed maximum if c_x, c_y and $\mathbf{Q}$ satisfy Eqs. (8) and (10). Thus, the equation for H_{c2} takes the form

$$
1 = \frac{4\phi_0 T\lambda}{vH\sqrt{\epsilon_\theta}} \mathrm{Re} \sum_{\omega>0}^{\Omega} \int_0^\infty \tan^{-1} \frac{v\sqrt{k^2 + \epsilon Q_z^2/\epsilon_\theta}}{2(\omega + i\mu H)}
$$
$$
\times \exp\left[-\frac{\phi_0 k^2}{2\pi H\sqrt{\epsilon_\theta}}\right] \frac{k\,dk}{\sqrt{k^2 + \epsilon Q_z^2/\epsilon_\theta}}. \qquad (11)
$$

The angular-dependent factor ϵ_θ describes the reduction of orbital pair breaking as $\mathbf{H}$ is rotated away from the c axis. If the Zeeman energy μH is negligible, Eq. (11) gives the GL angular scaling $H_{c2}(\theta) = H_{c2}(0)\epsilon_\theta^{-1/2}$ Ref. 68. The fact that for a parabolic band, the GL scaling of $H_{c2}(\theta)$ is not limited to the region of $T \approx T_c$ but is valid for all temperatures was pointed out by Brison *et al.*[47] who used the WHH approach.[35] Prohammer and Carbotte[69] arrived at the same conclusion by analyzing the Eliashberg equations but using Eq. (5) with $c_x = 2\epsilon_\theta^{1/2}/(1+\epsilon_\theta^{1/2})$ and $c_y = 2/(1+\epsilon_\theta^{1/2})$ inconsistent with Eq. (8) and also giving the wrong limit $c_x/c_y = \sqrt{\epsilon}$ for $\theta = \pi/2$, where the scaling requires $c_x/c_y = \epsilon$.

The uniaxial anisotropy tends to enhance the c-axis component of $\mathbf{Q}$ in Eq. (11) because the heavy c-axis mass reduces the kinetic energy loss due to the FFLO oscillations if $\mathbf{Q}$ is directed along the c axis. As a result, $\mathbf{Q}$ remains nearly parallel to the c axis as $\mathbf{H}$ is rotated away from the c axis until $\mathbf{H}$ becomes parallel to the ab plane and $\mathbf{Q}$ swings from the c axis to the ab plane orientation as shown in Fig. 2.

Following WHH,[35] Eq. (11) can be recast in a convenient dimensionless form by adding and subtracting $2\pi T\sum_{\omega>0}^{\Omega}\omega^{-1}$. This expresses λ and Ω in terms of T_c and gives the equation for $H_{c2}(T,\theta)$ and $Q(T,\theta)$ taking into account both orbital and paramagnetic effects

$$
\ln t + U(t,b,q) = 0,
$$

$$
U(t,b,q) = 2e^{q^2} \mathrm{Re} \sum_{n=0}^{\infty} \int_q^\infty du\, e^{-u^2}, \qquad (12)
$$

$$
\left\{\frac{u}{n+1/2} - \frac{t}{\sqrt{b}}\tan^{-1}\left[\frac{u\sqrt{b}}{t(n+1/2) + i\alpha b}\right]\right\}, \qquad (13)
$$

where $t = T/T_c$ and

$$
b = \frac{\hbar^2 v^2 \epsilon_\theta^{1/2} H}{8\pi\phi_0 T_c^2}, \quad \alpha = \frac{4\mu\phi_0 T_c}{\hbar^2 v^2 \epsilon_\theta^{1/2}}, \quad q^2 = \frac{Q_z^2 \epsilon \phi_0}{2\pi H\epsilon_\theta^{3/2}}. \qquad (14)
$$

Here α is related to the Maki parameter by $\alpha_M \approx 1.845\alpha$, the FFLO transition occurring if $\alpha \gtrsim 1$. Shown in Fig. 3 is an example of $H_{c2}(T)$ and $Q(T)$ calculated from Eq. (12) for $\alpha = 2$. The dashed line shows H_{c2} for $Q = 0$.
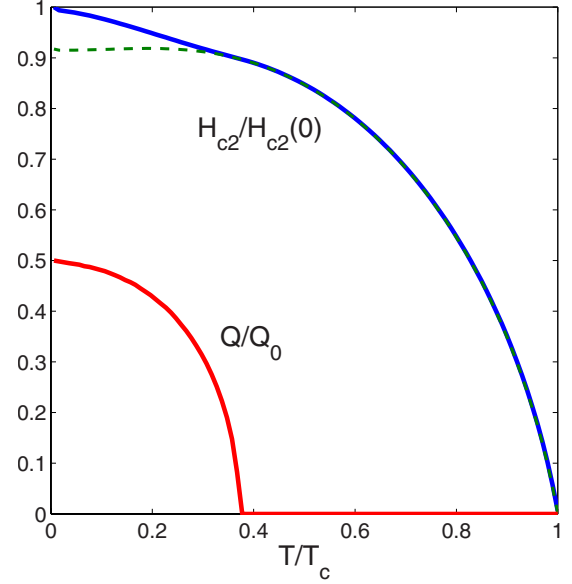
FIG. 3. (Color online) $H_{c2}(T)$ and $Q(T)$ calculated from Eqs. (12) and (13) for $\alpha = 2$ and $Q_0 = 2Q(0) \sim (4\pi k_B T_c/\hbar v)\sqrt{\epsilon_\theta/\epsilon}$.

Strong coupling effects can be taken into account in the square-well model of pairing interaction[69] by rescaling the Matsubara frequencies $\omega \to (1+\tilde{\lambda})\omega$ in Eq. (4). Here $\tilde{\lambda}$ is the electron-phonon coupling constant related to the BCS coupling constant by $\lambda = \tilde{\lambda} - \mu_e$, where μ_e is the Coulomb pseudopotential. As a result, the factors $(n+1/2)$ in Eq. (13) should be changed as follows:

$$
(n+1/2) \to (n+1/2)(1+\tilde{\lambda}), \qquad (15)
$$

The strong coupling effects change the FFLO instability criterion to $\alpha \gtrsim 1 + \tilde{\lambda}$ and increase the Zeeman pair-breaking field to $H_p = (1+\tilde{\lambda})H_p^{\mathrm{BCS}}$, where $\mu H_p^{\mathrm{BCS}} = \Delta/\sqrt{2}$ is the BCS paramagnetic limit.[70]

III. MULTIBAND CASE

Generalization of the approach presented in the previous section to multiband superconductors is straightforward although analytical results can only be obtained in a few special cases. The linearized equations for the order parameters $\Psi_m(\mathbf{r})$ on the mth sheet of the FS are given by the matrix version of Eq. (3)

$$
\Psi_l(\mathbf{r}) = \sum_m \int \Psi_m(\mathbf{r}')d^3\mathbf{r}' \int \frac{d^3\mathbf{k}}{(2\pi)^3} K_{lm}(\mathbf{k})
$$
$$
\times \exp\left[i\mathbf{k}(\mathbf{r}-\mathbf{r}') + \frac{i\pi}{\phi_0}\mathbf{H}\cdot(\mathbf{r}\times\mathbf{r}')\right], \qquad (16)
$$

where the matrix $K_{lm}(\mathbf{k})$ for ellipsoidal FSs is

$$
K_{lm} = \mathrm{Re}\sum_{\omega>0}^{\Omega} \frac{4\pi T\lambda_{lm}}{v_m\sqrt{p_\perp^2 + \epsilon_m p_z^2}}\tan^{-1}\frac{v_m\sqrt{p_\perp^2 + \epsilon_m p_z^2}}{2(\omega + i\mu H)}. \qquad (17)
$$

Here λ_{lm} is the matrix of pairing constants, the diagonal elements describing intraband pairing and the off-diagonal

components accounting for the interband interactions of $\Psi(\mathbf{r})$ on different FS sheets (hereafter no summation over repeated band indices is implied). If the Fermi velocities v_m and the mass anisotropy ratios ϵ_m are different for different bands, Eq. (5) no longer satisfies the multiband Eq. (16) because the parameters $\epsilon_{m\theta}$ and thus the scaling factors c_x and c_y in different bands are not equal to each other unless $\mathbf{H}\|c$. In this case the calculation of H_{c2} inclined by the angle θ with respect to the c axis requires expanding $\Psi_m(\mathbf{r})$ $=\Sigma_L C_{mL}\varphi_L(\mathbf{r})$ in a full set of oscillator eigenfunctions $\varphi_L(\mathbf{r})$, and Eq. (16) becomes the matrix equation both in the band indices m and s and the set of the oscillator quantum numbers L which account for all higher Landau levels.[26,27] In that regard the approach of Mansur and Carbotte,[71] who assumed $\Psi(\mathbf{r})$ of the form Eq. (5) with $Q=0$ and c_x and c_y from Ref. 69 separately for each band, gives an incorrect dependence of $H_{c2}(T,\theta)$ on θ based on the eigenfunctions, which do not satisfy Eq. (16).

In this paper we consider the simplest case of $\mathbf{H}\|c$ for which $\mathbf{Q}\|\mathbf{H}$, $\epsilon_{m\theta}=1$, and $c_x=c_y=1$ for all m, thus Eq. (5) is the solution of Eq. (16). Then H_{c2} is the maximum eigenvalue of the matrix $M_{lm}=\delta_{lm}-G_{lm}$

$$G_{lm} = \frac{\phi_0}{\pi H} \int_0^\infty K_{lm}(p)\exp\left[-\frac{\phi_0 p^2}{2\pi H}\right]p\,dp. \quad (18)$$

The effect of multiband pairing on the FFLO state and $H_{c2}(T)$ described by the equation $\mathrm{Det}\{M\}=0$ are addressed in the next section.

A. Two bands

In the case of two bands, Eq. (16) gives the equation for H_{c2}, which can be written in the following conventional form (see, e.g., Ref. 26)

$$a_1(\ln t + U_1) + a_2(\ln t + U_2) + (\ln t + U_1)(\ln t + U_2) = 0, \quad (19)$$

where $a_1=(\lambda_0+\lambda_-)/2w$, $a_2=(\lambda_0-\lambda_-)/2w$, $\lambda_-=\lambda_{11}-\lambda_{22}$, $\lambda_0=(\lambda_-^2+4\lambda_{12}\lambda_{21})^{1/2}$, and $w=\lambda_{11}\lambda_{22}-\lambda_{12}\lambda_{21}$. Here T_c is given by the well-known expression[72] valid for both $w>0$ and $w<0$

$$T_c = \frac{2\gamma}{\pi}\Omega\,\exp\left[\frac{\lambda_0-\lambda_+}{2w}\right], \quad (20)$$

where $\gamma=e^C\approx 1.78$ and $C=0.577$ is the Euler constant. Equation (19) has been used extensively to address the effects of multiband pairing on $H_{c2}(T)$ in MgB$_2$ for which the interband coupling constants are small: $\lambda_{12}\lambda_{21}\ll\lambda_{11}\lambda_{22}$. In the opposite limit of strong interband pairing $\lambda_{12}\lambda_{21}\gg\lambda_{11}\lambda_{22}$, which seems to be characteristic of ferropnictides, we have $a_1=a_2\rightarrow-1$ irrespective of the sign of λ_{12} and λ_{21}. The functions U_1 and U_2 are defined in the same way as in Eq. (12)

$$U_1 = 2e^{q^2}\,\mathrm{Re}\sum_{n=0}^{\infty}\int_q^\infty due^{-u^2},$$

$$\left\{\frac{u}{n+1/2}-\frac{t}{\sqrt{b}}\tan^{-1}\left[\frac{u\sqrt{b}}{t(n+1/2)+i\alpha b}\right]\right\}, \quad (21)$$

$$U_2 = 2e^{q^2 s}\,\mathrm{Re}\sum_{n=0}^{\infty}\int_{q\sqrt{s}}^\infty due^{-u^2},$$

$$\left\{\frac{u}{n+1/2}-\frac{t}{\sqrt{b\eta}}\tan^{-1}\left[\frac{u\sqrt{b\eta}}{t(n+1/2)+i\alpha b}\right]\right\}. \quad (22)$$

Here b, α, q, η, and s are defined as follows:

$$b = \frac{\hbar^2 v_1^2 H}{8\pi\phi_0 T_c^2}, \quad \alpha = \frac{4\mu\phi_0 T_c}{\hbar^2 v_1^2}, \quad (23)$$

$$q^2 = \frac{Q_z^2\phi_0\epsilon_1}{2\pi H}, \quad \eta = \frac{v_2^2}{v_1^2}, \quad s = \frac{\epsilon_2}{\epsilon_1}. \quad (24)$$

If the applicability condition of the Eliashberg theory $\Omega \ll E_F$ is satisfied for all bands, strong coupling effects can be taken into account by the rescaling of the Matsubara frequencies in K_{11} and K_{22}. In the square well model this yields $\omega \rightarrow\omega(1+\tilde{\lambda}_{11}+|\tilde{\lambda}_{12}|)$ in K_{11} and K_{12}, and $\omega\rightarrow\omega(1+\tilde{\lambda}_{22}+|\tilde{\lambda}_{21}|)$ in K_{22} and K_{21}.[69,70] The tilde marks the electron-boson coupling constants, $\lambda_{lm}=\tilde{\lambda}_{lm}-\mu_{lm}$, and μ_{lm} is the matrix of the Coulomb pseudopotentials. Here λ_{12} and λ_{21} satisfy the symmetry relation $N_1\lambda_{12}=N_2\lambda_{21}$, and N_1 and N_2 are partial densities of states in band 1 and 2, respectively. As a result, we arrive at Eqs. (19)–(22) in which the factors $n+1/2$ in U_1 and U_2 should be changed to

$$n+1/2 \rightarrow (n+1/2)(1+\tilde{\lambda}_{11}+|\tilde{\lambda}_{12}|), \quad (U_1), \quad (25)$$

$$n+1/2 \rightarrow (n+1/2)(1+\tilde{\lambda}_{22}+|\tilde{\lambda}_{21}|), \quad (U_2). \quad (26)$$

Currently little is known about the values of $\tilde{\lambda}_{lm}$ and μ_{lm} in pnictides so to reduce the number of parameters in the subsequent analysis, the renormalization defined by Eqs. (25) and (26) is disregarded.

Summing over n in Eqs. (21) and (22) as described in Appendix B, yields

$$U_1 = \ln(4\gamma) + \frac{te^{q^2}}{\sqrt{b}}\int_q^\infty due^{-u^2}\times\mathrm{Im}\,\ln\frac{\Gamma[1/2+i(\alpha b+u\sqrt{b})/t]}{\Gamma[1/2+i(\alpha b-u\sqrt{b})/t]}, \quad (27)$$

where $\Gamma(x)$ is the gamma function and U_2 is obtained by rescaling $\sqrt{b}\rightarrow\sqrt{\eta b}$ in Eq. (27) except the terms $\propto\alpha b$. Several limiting cases can be calculated analytically. If $T\approx T_c$, the U functions can be expanded in $b\ll 1$ and $\tau=(T_c-T)/T_c\ll 1$ (Appendix B). To see the role of paramagnetic effects, we also retain the quadratic terms $\sim\alpha^2 b^2$, which are only essential if $\alpha\gtrsim 1$. Then

$$b_{c2} = \frac{1}{6\alpha^2}[\sqrt{c_0^2 + 36\alpha^2\tau/7\zeta(3)} - c_0], \quad (28)$$

where $c_0=c_++\eta c_-$, $2c_\pm=1\pm\lambda_-/\lambda_0$, and $\zeta(3)\approx 1.202$. For $\alpha<1$, Eq. (28) yields
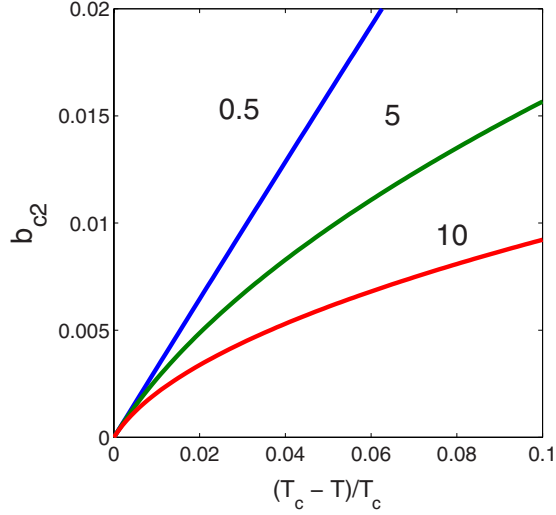
FIG. 4. (Color online) $H_{c2}(T)$ calculated from Eq. (28) for different values of α and $\eta=0.1$.

$$H_{c2}(T) = \frac{24\pi\phi_0 T_c(T_c - T)}{7\zeta(3)\hbar^2(c_+ v_1^2 + c_- v_2^2)}, \quad \alpha < 1 \qquad (29)$$

For identical bands, ($v_1 = v_2 = v$, $\lambda_{11} = \lambda_{22}$, and $c_+ = c_- = 1/2$), Eq. (29) reduces to the single-band GL expression, $H_{c2} = \phi_0/2\pi\xi^2$, where $\xi = (\hbar v/k_B\pi)[7\zeta(3)/48T_c(T_c - T)]^{1/2}$ is the coherence length in the clean limit.[68] For the $s^\pm$ pairing ($c_+ \to c_- \to 1/2$), the dependence of $H_{c2}(T)$ on the materials parameters resembles $H_{c2}(T)$ in the s^{++} dirty limit: for strong band asymmetry ($\eta \ll 1$ or $\eta \gg 1$), H_{c2} in Eq. (29) is limited by the band with *larger* Fermi velocity, similar to H_{c2} mostly limited by the band with larger diffusivity for the s^{++} case.[26] Paramagnetic effects increase the slope of $H_{c2}(T)$ and reduce the effect of band asymmetry. For $\alpha \gg 1$, Eq. (28) yields

$$H_{c2} = \frac{2\pi[T_c(T_c - T)]^{1/2}}{\mu\sqrt{7\zeta(3)}}, \quad \alpha^2\tau \gg 1. \qquad (30)$$

Here $H_{c2}(T)$ is insensitive to the band parameters, both $s^\pm$ and s^{++} models giving the same $H_{c2}(T)$ near T_c. The behavior of $H_{c2}(T)$ for different values of α is shown in Fig. 4: close to T_c all $H_{c2}(T) \propto T_c - T$ are linear, changing to $H_{c2} \propto \sqrt{T_c - T}$ for large α as T is decreased.

For $T \ll T_c$, one can use the asymptotic of $\ln\Gamma(z) = (z - 1/2)\ln z - z$ at $z \gg 1$ (Ref. 73) in Eq. (27) equivalent to the replacement of the n summation in Eqs. (21) and (22) by integration. Strictly speaking, this cannot be used for $\Gamma(u)$ in the denominator of Eq. (27) at $u = \alpha\sqrt{b}$ but the resulting logarithmic singularity gives a negligible contribution to the integral in Eq. (27) at $t \to 0$. The equation for H_{c2} at $T=0$ is given by Eq. (19) in which the combinations $D_m = \ln t + U_m$ become temperature-independent integrals calculated in Appendix B. For $T=0$ and arbitrary b and α, the formulas for D_1 and D_2 are such that Eq. (19) cannot be solved analytically but if $\alpha \ll 1$ they simplify to $D_1 = \frac{1}{2}\ln(16\gamma b) - 1$ and $D_2 = D_1 + \frac{1}{2}\ln\eta$. In this case Eq. (19) becomes a quadratic equation for D_1, giving the explicit expression for $H_{c2}(0)$
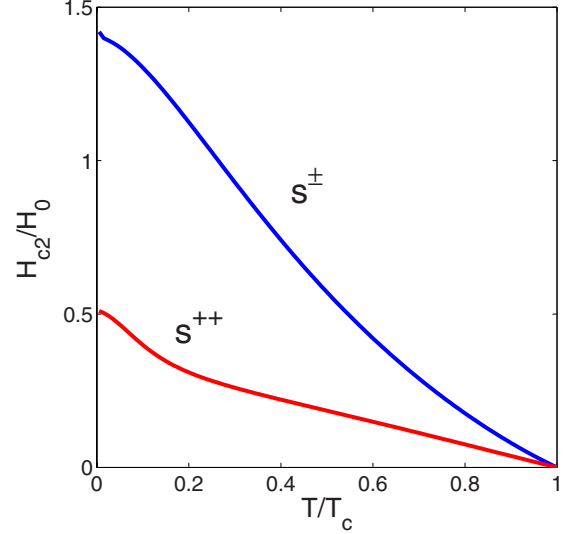
FIG. 5. (Color online) Comparison of $H_{c2}(T)$ curves for $s^\pm$ and s^{++} pairings and $\alpha=0$, where $H_0 = 8\pi\phi_0 k_B^2 T_c^2/\hbar^2 v_1^2$. The $s^\pm$ case was calculated for $\lambda_{12}\lambda_{21} = 0.25$ and $\eta=0.01$. The s^{++} case was calculated for $\eta=0.01$ and λ_{lm} of MgB$_2$: $\lambda_{11}=0.81$, $\lambda_{22}=0.29$, $\lambda_{12}=0.13$, and $\lambda_{21}=0.09$ taken from Ref. 75.

$$H_{c2} = \frac{e^2\pi\phi_0 T_c^2}{2\gamma\hbar^2 v_1 v_2}\exp(g), \quad \alpha \ll 1, \qquad (31)$$

$$g = \frac{w}{|w|}\left[\frac{\lambda_0^2}{w^2} + \frac{\lambda_-}{w}\ln\eta + \frac{\ln^2\eta}{4}\right]^{1/2} - \frac{\lambda_0}{w}, \qquad (32)$$

where $e \approx 2.718$ and the factor $w/|w|$ selects the correct branch of the solution as w changes sign. For $v_1 = v_2 = v$, Eq. (31) gives $H_{c2}(0) = e^2\pi\phi_0 T_c^2/2\gamma\hbar^2 v^2$, the same as $H_{c2}(0)$ for a clean single-band superconductor.[35,74] However, strong band asymmetry affects $H_{c2}(0)$ for the $s^\pm$ and s^{++} cases very differently. For the s^{++} pairing at $|\ln\eta| \gg 2\lambda_0/w$, the value of $H_{c2}(0) \propto v_2^{-2}$ is limited by the *smaller* Fermi velocity in band 2, and $H_{c2}(0)$ is cut off by the paramagnetic pair breaking and interband impurity scattering as $v_2 \to 0$.[26] By contrast, $H_{c2}(0)$ for the $s^\pm$ pairing is limited by the *larger* Fermi velocity in band 1 and tends to a finite value as $v_2 \to 0$

$$H_{c2}(0) \to \frac{e^2\pi\phi_0 T_c^2}{2\gamma\hbar^2 v_1^2}e^{(\lambda_0 + \lambda_-)/|w|} = \frac{2\gamma e^2\phi_0\Omega^2}{\pi\hbar^2 v_1^2}e^{2\lambda_{11}/|w|},$$
$$\qquad (33)$$

where Eq. (20) was used.

Shown in Fig. 5 is the comparison of $H_{c2}(T)$ calculated for $\alpha=0$ and $\eta=0.01$ for the $s^\pm$ and s^{++} scenarios. In both cases the band asymmetry results in convex $H_{c2}(T)$ curves. For the s^{++} case, $H_{c2}(T)$ has a low-T upturn well documented for dirty MgB$_2$ (Ref. 26) while $H_{c2}(T)$ for the $s^\pm$ case exhibits an upward curvature at intermediate temperatures, consistent with the high-field measurements on pnictides.[10,11] Notice that the magnitude of H_{c2} for the $s^\pm$ case is about three times larger than for the s^{++} case, consistent with very high H_{c2} of ferropnictides. Although $H_{c2}(0) \propto 1/v_1^2$ for the $s^\pm$ case is limited by the larger Fermi velocity v_1, the band asymme-

try can strongly [by the factor $\sim(\Omega/T_c)^2 \gg 1$] enhance $H_{c2}(0)$. In turn, this increases the Maki parameter $\alpha_M \sim \mu H_{c2}/T_c$, facilitating the FFLO transition, as shown in the next section.

B. Multiband FFLO state

FFLO state in multiband superconductors can be rather different from that of the single band superconductors if the FFLO instability occurs only in one band. We mostly focus here on the case of strong interband coupling for the $s^{\pm}$ pairing, for which $w=\lambda_{11}\lambda_{22}-\lambda_{12}\lambda_{21}<0$ and the FFLO instability occurs at much smaller intraband Maki parameters than for weak interband coupling $w>0$ characteristic of the s^{++} superconductivity in MgB$_2$. If the chemical potential is shifted by doping or irradiation, one of the FS pockets shrinks and the other expands, thus the shrinking FS of band 2 may trigger the phase locked FFLO oscillations $\Psi_1 \propto \Psi_2 \propto \exp(iQz)$ in both bands as α_2 is increased. The FFLO state in one band only is impossible because it would average the interband coupling energy to zero, resulting in the energy loss of the order of the condensation energy. However, enforcing the global FFLO state increases the kinetic energy in band 1 with $\alpha_1<1$ which damps the FFLO instability. Because the increase of the FFLO kinetic energy is proportional to $\epsilon_1 Q^2$, such damping by band 1 is reduced by uniaxial anisotropy if $\epsilon_1 \ll 1$.

The FFLO transition is therefore facilitated if one weakly anisotropic FS pocket is above the FFLO threshold while another anisotropic FS pocket is below the FFLO threshold. This is illustrated in Figs. 6(a)–6(c) which show the results of numerical simulations of Eqs. (19)–(22) for $\alpha_2 =4\mu\phi_0 T_c/\hbar^2 v_2^2=5$, $\eta=0.1$, and $\alpha_1=4\mu\phi_0 T_c/\hbar^2 v_1^2=0.5$. For the case of strong anisotropy, $\epsilon_1=0.01$ represented by Fig. 4(a), $H_{c2}(T)$ and $Q(T)$ exhibit behaviors similar to that shown in Fig. 3 for a single band superconductor. This is not surprising given that for $\epsilon_1 \ll \epsilon_2$, the FFLO state is mostly controlled by the band 2 while the FFLO damping by band 1 is reduced by the effect of anisotropy. As the mass anisotropy ratio $s=\epsilon_2/\epsilon_1$ decreases, the band with $\alpha_1<1$ hinders the FFLO instability, shifting the region where $Q>0$ to lower T and eventually suppressing the FFLO state as s further decreases.

Figures 6(a)–6(c) reveal another feature of multiband superconductors: while the $H_{c2}(T)$ curve in Fig. 6(a) has the characteristic low-T upturn indicative of the FFLO state, $H_{c2}(T)$ for the less anisotropic case in Fig. 6(b) would be hard to distinguish from the conventional single-band WHH behavior for which paramagnetic effects flatten $H_{c2}(T)$ at low T. Yet the FFLO state for the case shown in Fig. 6(b) does exist, but $H_{c2}(T)$ for $Q>0$ at low T is only slightly higher than $H_{c2}(T)$ for $Q=0$. Such "hidden" FFLO state is even more difficult to reveal from the analysis of $H_{c2}(T)$ curves as the parameters α_1 and α_2 further decrease. This is illustrated by Figs. 7(a)–7(c), which show $H_{c2}(T)$ and $Q(T)$ calculated from Eq. (19) for $\alpha_2=2$ and $\alpha_1=0.2$. In this case all $H_{c2}(T)$ curves look very WHH-like and do not even exhibit the apparent paramagnetic flattening of $H_{c2}(T)$ at low T, yet the FFLO state still exists here for the cases (a) and (b).
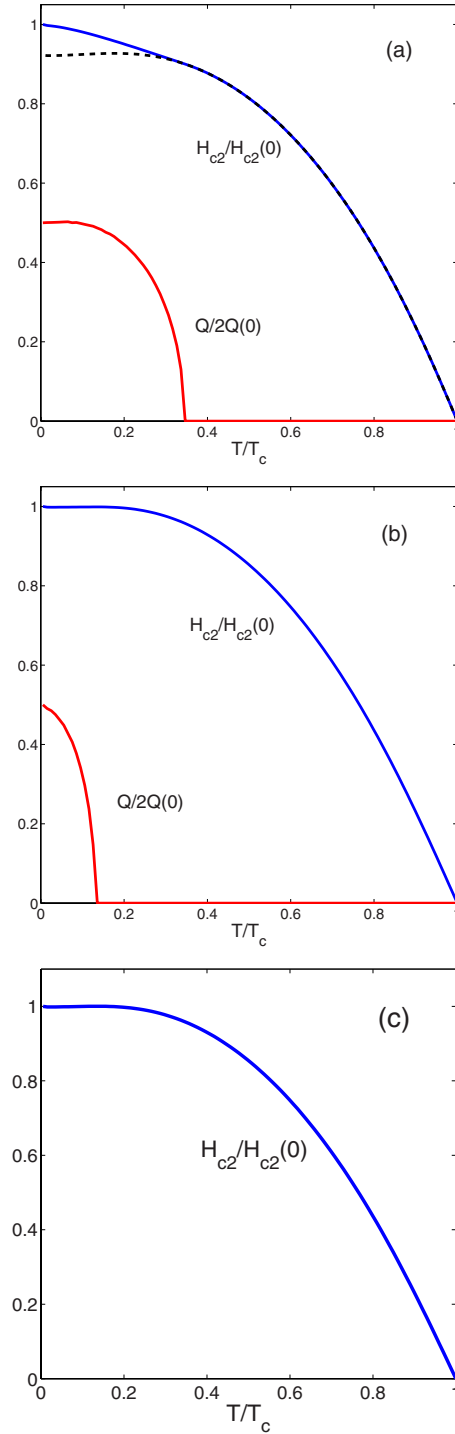
FIG. 6. (Color online) $H_{c2}(T)$ and $Q(T)$ calculated from Eqs. (19)–(22) for $\alpha=0.5$, $\lambda_{12}\lambda_{21}=0.25$, $\lambda_{11}=\lambda_{12}=0$ and $\eta=0.1$, and different values of ϵ: (a) 0.01; (b) 0.5, and (c) 1. Here the dashed line in (a) shows $H_{c2}(T)$ for $Q=0$. Although the FFLO state exists in (b), the curves $H_{c2}(T,Q)$ and $H_{c2}(T,0)$ become nearly indistinguishable so $H_{c2}(T,0)$ is not shown.

It is interesting to compare the behavior of $H_{c2}(T)$ and $Q(T)$ in $s^{\pm}$ and s^{++} superconductors. An example of the latter is MgB$_2$ for which $w>0$ and $\lambda_{12}\lambda_{21} \ll \lambda_{11}\lambda_{22}$. Calculations using Eqs. (19)–(22) and $\lambda_{11}=0.81$, $\lambda_{22}=0.29$, $\lambda_{12}=0.13$, and $\lambda_{21}=0.09$ for a clean MgB$_2$ (Ref. 75) give the overall behav-
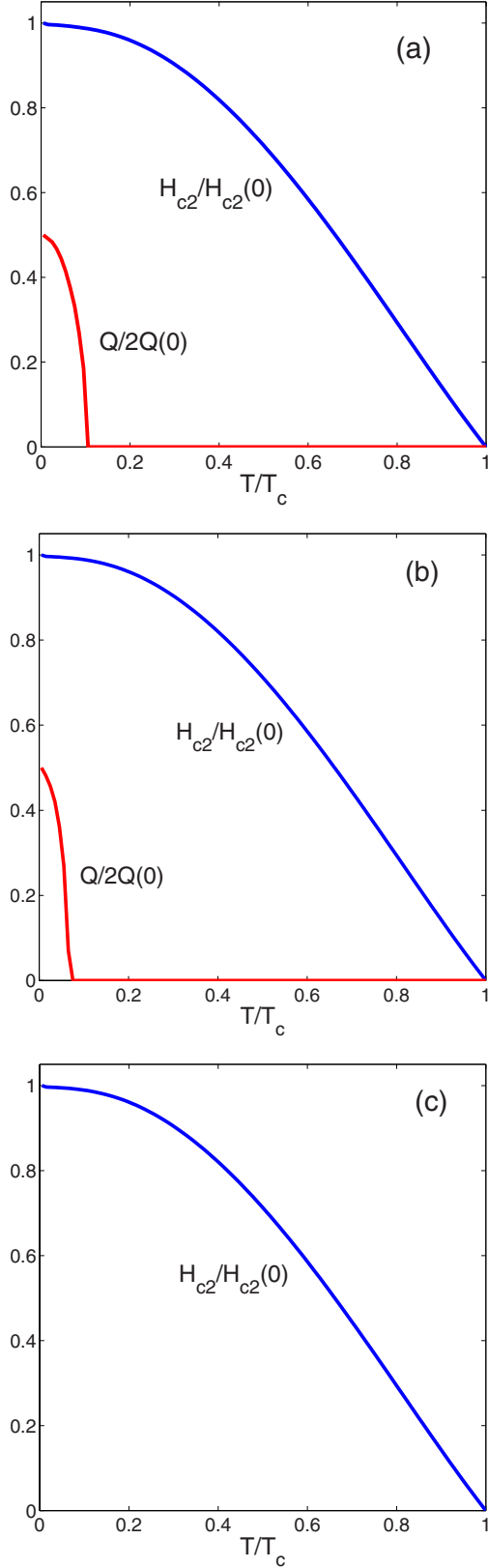
FIG. 7. (Color online) $H_{c2}(T)$ and $Q(T)$ calculated from Eqs. (19)–(22) for $\alpha=0.2$, $\lambda_{12}\lambda_{21}=0.25$, $\lambda_{11}=\lambda_{22}=0$, and $\eta=0.1$, and different values of ϵ: (a) 0.01; (b) 0.05, and (c) 0.1. Here $H_{c2}(T,0)$ for $Q=0$ is not shown because for these parameters the curves $H_{c2}(T,Q)$ and $H_{c2}(T,0)$ are nearly indistinguishable although the FFLO state does exist in (a) and (b).
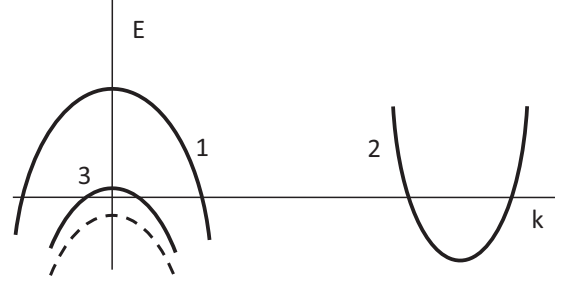
FIG. 8. The emerging FS hole pocket 3 moving from the position below the Fermi level (dashed) to the position above the Fermi level upon a small shift of the chemical potential.

ior of $H_{c2}(T)$ and $Q(T)$ similar to that is shown in Fig. 7 but with a significantly narrower range of the parameters where the FFLO state can exist. For example, for $\alpha_1=0.5$ and $\eta=0.1$ in Fig. 6, the FFLO state for the s^{++} pairing disappears below the critical anisotropy parameter $s<s_c\approx0.035$, about 20 times smaller than for the $s^{\pm}$ case.

C. FFLO state caused by emerging FS pocket

Here we consider the FFLO instability in multiband superconductors due to opening up a new FS pocket upon a small shift of the chemical potential. This situation may be relevant to ferropnictides in which several bands with large effective masses are often situated just slightly below the Fermi level at or close to the optimal doping,[52–54] as depicted in Fig. 8. Because of a large intraband Maki parameter $\alpha_M \propto 1/E_F$ for the emerging FS pocket, the small shift of the chemical potential can trigger the global FFLO instability ameliorated by strong uniaxial anisotropy of the main bands 1 and 2. We illustrate this effect assuming the $s^{\pm}$ model and neglecting all intraband (diagonal) components of λ_{lm}. Then the gap Eqs. (16) and (17) take the form

$$\Delta_1 = \lambda_{12}\widetilde{K}_2\Delta_2, \quad \Delta_3 = \lambda_{32}\widetilde{K}_2\Delta_2, \quad (34)$$

$$\Delta_2 = \lambda_{21}\widetilde{K}_1\Delta_1 + \lambda_{23}\widetilde{K}_3\Delta_3, \quad (35)$$

where $G_{lm}=\lambda_{lm}\widetilde{K}_{lm}$. The equation for H_{c2} becomes

$$1 = \lambda_{12}\lambda_{21}\widetilde{K}_1\widetilde{K}_2 + \lambda_{23}\lambda_{32}\widetilde{K}_2\widetilde{K}_3. \quad (36)$$

It is convenient to rewrite Eq. (36) in terms of the U functions, using $\widetilde{K}_m=\ln(2\gamma\Omega/\pi T_c)-\ln t-U_m$, and expressing $T_c=\Omega\exp(-1/\lambda)$ in terms of the effective coupling constant $\lambda=(\lambda_{12}\lambda_{21}+\lambda_{23}\lambda_{32})^{1/2}$. Then Eq. (36) can be recast in the two-band form

$$\lambda(\ln t + \widetilde{U}_1)(\ln t + U_2) = 2\ln t + \widetilde{U}_1 + U_2, \quad (37)$$

$$\widetilde{U}_1 = \frac{U_1 + gU_3}{1+g}, \quad g = \frac{\lambda_{23}\lambda_{32}}{\lambda_{21}\lambda_{12}}. \quad (38)$$

Redefining $\widetilde{U}_1 \to U_1$ and $\lambda \to |w|/\lambda_0$ turns Eq. (37) into Eq. (19) in the limit $\lambda_{12}\lambda_{21} \gg \lambda_{11}\lambda_{22}$ for which $a_1=a_2\to-1$. Therefore, the effect of the emerging FS pocket can be
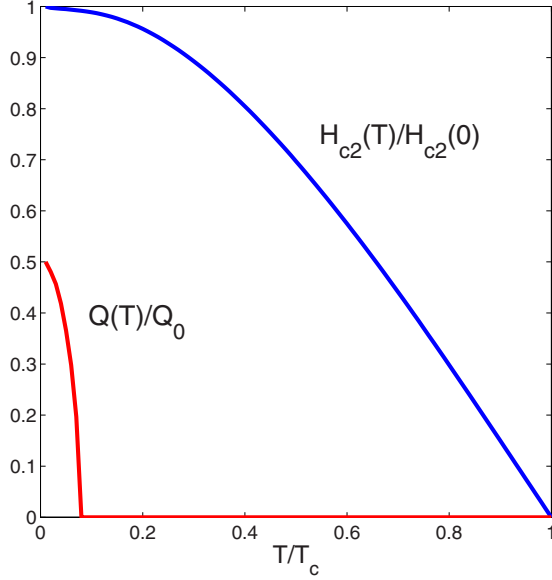
FIG. 9. (Color online) $H_{c2}(T)$ and $Q(T)$ calculated from Eq. (37) for $\alpha=0.3$, $\lambda=0.5$, $g=0.2$, $s=50$, $\eta=0.04$, and $Q_0=2Q(0)$.

treated in the above two-band scheme but with the replacement of U_1 with the effective $\widetilde{U}_1$. Since the parameters of the main bands 1 and 2 do not change much upon a small shift of the chemical potential, the emerging FS pocket with large $\alpha_3 \propto 1/E_F$ may trigger the FFLO instability without significant effect on T_c.

To reduce the number of model parameters in the subsequent discussion, we assume nesting of bands 1 and 2, so that $U_1=U_2$, and $\lambda_{lm}=V_{lm}N_m$ with only two interband matrix elements V_{12} and V_{32} between bands 1 and 2 and 3. In this model g is given by

$$g = \frac{N_3 V_{32}^2}{N_1 V_{12}^2} = \frac{m_3^2 V_{32}^2}{m_1^2 V_{12}^2} \sqrt{\frac{\eta}{s}}, \qquad (39)$$

where $\eta=(v_3/v_1)^2$ and $s=\epsilon_3/\epsilon_1$.

Shown in Fig. 9 are $H_{c2}(T)$ and $Q(T)$ calculated from Eqs. (37) and (38) assuming a moderate value of $\alpha=0.3$ in the main bands 1 and 2 and other parameters given in the caption. As the anisotropy ratio s decreases, the $H_{c2}(T)$ and $Q(T)$ curves evolve in the same way as those shown in Figs. 6 and 7. Similar to the two-band case, the FFLO state also disappears as s becomes smaller than a critical value obtained from the numerical solutions of Eq. (11) for a given set of parameters and the $H_{c2}(T)$ curve [such as those shown in Figs. 6(a) and 6(b)] does not exhibit visible changes below the FFLO instability threshold. The latter indicates that the critical lines $H_{c2}[T,Q(T)]$ and $H_{c2}(T,0)$ are rather close.

D. Effect of doping on the multiband FFLO state

The way the FFLO state appears upon doping can be traced using Eqs. (37) in which the ratio $\eta=(v_3/v_1)^2$ proportional to the Fermi energy of the emerging FS pocket is regarded as a control parameter. It is assumed that $\eta \ll 1$ so

small variations of the electronic parameters of bands 1 and 2 upon doping are neglected, except for the change in the pairing constant

$$\lambda = \lambda_0 \sqrt{1+g} \simeq \lambda_0(1+g/2), \qquad (40)$$

where $\lambda_0=(\lambda_{12}\lambda_{21})^{1/2}$ and the coupling parameter $g<1$ is given by Eq. (39). If $\eta \rightarrow 0$ the FS pocket has a large Maki parameter but small density of states so it is coupled weakly ($g \ll 1$) with the main bands 1 and 2 which suppress the FFLO instability. Since $g \propto \sqrt{\eta}$, the FFLO state therefore first appears above the critical value $\eta > \eta_c$ at $T=0$. We calculate η in the model with $U_1=U_2$ for which Eqs. (37) at $T=0$ reduce to

$$\lambda(g)(D+gD_i)D = (2+g)D + gD_i. \qquad (41)$$

Here the functions $D=\ln t+U_1$ and $D_i=\ln t+U_3$ in the limit of $t \rightarrow 0$ were calculated in Appendix B

$$D = C - 1 + \frac{1}{2}\ln(16b) + e^{q^2}\int_q^\infty du e^{-u^2},$$

$$[(u+\alpha\sqrt{b})\ln(u+\alpha\sqrt{b}) + (u-\alpha\sqrt{b})\ln|u-\alpha\sqrt{b}|], \quad (42)$$

$$D_i = C - 1 + \frac{1}{2}\ln(16b\eta) + e^{q^2s}\int_{q\sqrt{s}}^\infty du e^{-u^2},$$

$$[(u+\alpha_i\sqrt{b})\ln(u+\alpha_i\sqrt{b}) + (u-\alpha_i\sqrt{b})\ln|u-\alpha_i\sqrt{b}|], \quad (43)$$

where $\alpha_i=\alpha/\sqrt{\eta}$. Equations (41)–(43) define the dependencies of $H_{c2}(T,Q)$ and $Q(T)$ at $T=0$. The critical value η_c is obtained by differentiating Eq. (41) with respect to q^2 under the condition $\partial_q b=0$ at $q \rightarrow 0$

$$\lambda(2DD' + gD'D_i + gD_i'D) = (2+g)D' + gD_i', \quad (44)$$

where the prime denotes $\partial_{q^2}|_{q \rightarrow 0}$. Excluding b from Eqs. (41) and (44) gives the equation for η_c as a function of materials parameters.

Shown in Fig. 10 are examples of $\eta_c(\alpha)$ calculated for different values of the parameter s. For $\alpha \rightarrow 1$, both bands 1 and 2 are close to the FFLO instability so the emerging FS pocket with $\alpha_i=\alpha/\sqrt{\eta}$ would always trigger the global FFLO instability at $\eta_c \rightarrow 0$. As α decreases, $\eta_c(\alpha)$ increases, reaching the end point at $\alpha=\alpha_m$ where $\partial_\alpha \eta_c \rightarrow \infty$. Consistent with the results of the previous sections, the increase of the anisotropy parameter s decreases η_c. Figure 10 shows that the FFLO transition can only occur if α for the main bands 1 and 2 is within the parameter window $\alpha_m < \alpha < 1$, where α_m corresponds to the end point of the solid curve $\eta_c(\alpha)$. Here the emerging FS pocket, while not affecting global superconducting properties, can nevertheless reduce the FFLO instability threshold, the effect becoming more pronounced as s increases, for example, $\alpha_m \simeq 0.47$ for $s=10$ and $\alpha_m \simeq 0.38$ for $s=25$ in Fig. 10. These cases correspond to moderate Maki parameters for which the manifestations of paramagnetic effects are not really apparent in the observed $H_{c2}(T)$. For $\alpha \simeq 0.3$–0.5, the shape of $H_{c2}(T)$ remains WHH-like with no visible low-T upturn, yet the FFLO state facilitated by the $s^{\pm}$ pairing and the uniaxial anisotropy does occur here at low T.
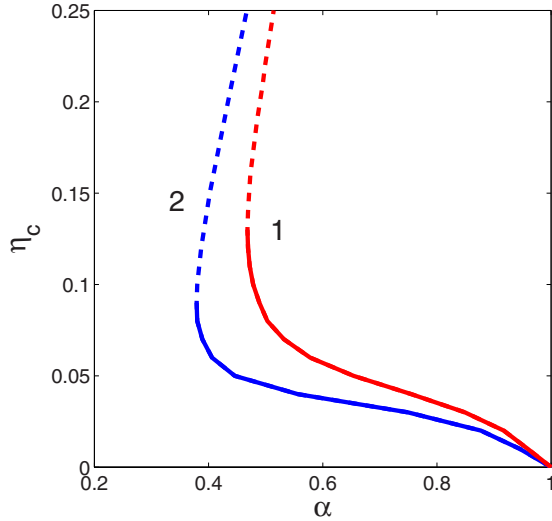
FIG. 10. (Color online) The critical value η_c calculated from Eqs. (41) for $m_3 = 2m_1$ and $s = 25$ (1) and $s = 10$ (2). The dashed curves show unstable branches of $\eta_c(\alpha)$.

The above model is based on the quasiclassical first Landau level wave function in Eq. (5), which may still be applicable if $\alpha_i = \alpha/\sqrt{\eta}$ is not very big. For larger $\alpha_i \gtrsim 9$, quantum effects become essential and higher Landau levels should be taken into account.[47,67,76] Therefore for small $\eta \lesssim (\alpha/9)^2$, quantum oscillations in $H_{c2}(T)$ (Refs. 76 and 77) caused by the FS pocket may appear.

IV. DISCUSSION

The results of this work show that the $s^\pm$ multiband pairing can result in upward curvature of $H_c(T)$ parallel to the c axis in intermediate temperature range. This behavior is different from the characteristic low-T upturn of $H_{c2}(T)$ for the s^{++} order parameter in MgB$_2$,[26] as illustrated by Fig. 5. The $s^\pm$ scenario is therefore more consistent with the measurements of $H_{c2}(T)$ on Nd-1111 single crystals[11] which do exhibit the upward curvature at intermediate T. Moreover, as shown in Sec. III, the $s^\pm$ pairing significantly enhances the orbitally limited H_{c2} as compared to the s^{++} case (see also Fig. 5), consistent with very high H_{c2} of ferropnictides. The $s^\pm$ pairing thus facilitates the FFLO transition.

The $s^\pm$ FFLO state may not be apparent from the analysis of $H_{c2}(T)$ curves unlike the single-band case FFLO upturn in $H_{c2}(T)$ at low T (see Fig. 3), which has been observed on CeCoIn$_5$ (Refs. 37–40) and organic superconductors.[41–43] The multiband $s^\pm$ FFLO state can exhibit a similar $H_{c2}(T)$ upturn [see Fig. 6(a)] but also have a conventional WHH-like shape,[35] as illustrated in Figs. 7 and 9. This results from competition of the band with $\alpha > \alpha_c$ which tends to enforce the FFLO state and the shape of $H_{c2}(T)$ similar to that shown in Fig. 3, and the band with $\alpha < \alpha_c$ for which $H_{c2}(T)$ mostly limited by orbital effects. The resulting mixture of two behaviors can produce $H_{c2}(T)$ curves similar to what would be normally expected from orbital pair breaking only, even if the FFLO state does exist at low T. Such a hidden FFLO transition results from the reduction in the damping effect of

the band with $\alpha < \alpha_c$ by uniaxial anisotropy, which makes the critical fields $H_{c2}(T, Q=0)$ and $H_{c2}(Q)$ very close. As a result, the detection of the FFLO state from transport measurements at high fields becomes rather difficult so other techniques such as the measurements of latent heat at the first-order FFLO phase transition,[37] torque magnetometry or fluctuation contributions to the specific heat, paraconductivity or magnetic susceptibility at high fields[78,79] may be more suitable to reveal the FFLO state in ferropnictides.

The multiband $s^\pm$ pairing with several "shadow" bands close to the FS in ferropnictides can result in the FFLO state caused by a small shift of the chemical potential which opens up a new FS pocket. This may enable one to tune the FFLO state by doping or by irradiation,[80] which could provide the necessary shift of E_F without introducing too much disorder which would suppress T_c and the FFLO instability.[35] This feature could also be used to reveal quantum oscillations in $H_{c2}(T)$ produced by the emerging FS pocket.

The effect of anisotropy can change the temperature dependence of $H_{c2}(T)$ as **H** is rotated away from the c axis. For the s^{++} pairing, this manifests itself in the change from convex $H_{c2}(T)$ curves at **H**$\|c$ to concave $H_{c2}(T)$ curves at **H**$\|ab$, as has been observed in MgB$_2$.[26] Calculation of H_{c2} for incline field in the clean limit is more complicated, as it requires expansion of Ψ in the full set of oscillator wave functions and then finding a maximum eigenvalue H_{c2} of an infinite matrix in both the band indices and the Landau level quantum numbers. Qualitatively, one could still use Eq. (5) as a variational trial function for an inclined field, which results in Eq. (19) for $H_{c2}(T, \theta)$ where U_1 and U_2 depend on the intraband parameters $\epsilon_1(\theta)$ and $\epsilon_2(\theta)$, respectively, such as in Eqs. (13) and (14), and c_x, c_y, Q_y, and Q_z are to be found self-consistently from the maximum of H_{c2}.

The effect of anisotropy on the $s^\pm$ FFLO state can be quite complex. On the one hand, rotating **H** toward the ab plane increases H_{c2}, which would expand the region of T where FFLO state exists. Thus, the parallel field orientation **H**$\|ab$ is the most beneficial for the FFLO state in a single band superconductor. On the other hand, rotating **H** away from the c axis in multiband superconductors increases the kinetic energy term $\epsilon_1 Q_z^2/\epsilon_1(\theta)$ in U_1, which enhances the dumping of the FFLO instability by band 1, and thus reducing the range of temperatures where the FFLO state can exist. The competition of these opposite trends could produce an intricate dependence of the FFLO instability on the materials parameters.

An interesting situation may result from the effect of anisotropy on vortices in the FFLO state. As was shown in Sec. II, the wave vector **Q** is not parallel to **H** in a uniaxial superconductor for which **Q** in the case of strong mass anisotropy $\epsilon = m/m_c \ll 1$ remains nearly parallel to the c axis practically for all field orientations except **H** almost parallel to the ab planes (see Fig. 2). The component Q_y perpendicular to the vortex lines facilitates the appearance of metastable fractional vortices, as has been shown in the case when Q_y was induced by the FFLO state in single band noncentrosymmetric superconductors[81] or cold atoms.[82] Such fractional vortices may be more energetically favorable than the conventional Abrikosov lattice in a certain range of materials parameters and H close to H_{c2}.[81] As our results indicate,

similar fractional vortex structures might occur in single-band uniaxial superconductors in inclined fields but generalization of these results to multiband anisotropic superconductors remains open.

APPENDIX A: TRANSFORMATION OF THE EQUATION FOR H_{c2} TO ISOTROPIC FORM

To obtain the equation for H_2 we multiply Eq. (3) by $\Psi^*(\mathbf{r})$ and integrate over $\mathbf{r}$ and $\mathbf{r}'$

$$\frac{\pi}{2h\sqrt{c_x c_y}} = \int \frac{d^2\mathbf{k}}{(2\pi)^2} d^2\mathbf{r}' d^2\mathbf{r} \widetilde{K}(\mathbf{k}) \exp[i\mathbf{t}(\mathbf{r} - \mathbf{r}') + 2ih(xy')$$
$$- yx') - hc_x(x^2 + x'^2) - hc_y(y^2 + y'^2)], \quad (A1)$$

where $\widetilde{K}(\mathbf{k}) = K(k_x, k_y, Q_z)$ as the z integration gives $2\pi\delta(k_z - Q_z)$, $\mathbf{t} = \mathbf{k} - \mathbf{Q}_\perp$, and $\mathbf{Q}_\perp$ is a projection of $\mathbf{Q}$ onto the xy plane. The xy integration is done using

$$\int d^2\mathbf{r} \exp[i\mathbf{tr} + 2ih(xy' - yx') - hc_x x^2 - hc_y y^2]$$
$$= \frac{\pi}{h\sqrt{c_x c_y}} \exp\left[-\frac{(t_x + 2hy')^2}{4hc_x} - \frac{(t_y - 2hx')^2}{4hc_y}\right]. \quad (A2)$$

Integrating then over $d^2\mathbf{r}'$ in Eq. (A1) yields

$$1 = \frac{\sqrt{c_x c_y}}{2\pi h(c_x c_y + 1)} \int d^2\mathbf{k} \widetilde{K}(\mathbf{k})$$
$$\times \exp\left[-\frac{c_y(k_x - Q_x)^2}{2h(c_x c_y + 1)} - \frac{c_x(k_y - Q_y)^2}{2h(c_x c_y + 1)}\right], \quad (A3)$$

where the wave vector $\mathbf{k}$ in the field frame is related to the wave vector $\mathbf{p}$ in the crystal frame by: $k_x = p_x$ and

$$p_y = k_y \cos\theta + Q_z \sin\theta, \quad (A4)$$

$$p_z = Q_z \cos\theta - k_y \sin\theta. \quad (A5)$$

For an anisotropic parabolic band, $\widetilde{K}(\mathbf{p})$ depends only on the combination $R = p_x^2 + p_y^2 + \epsilon p_z^2$, which can be transformed into the isotropic form $\widetilde{R} = \widetilde{k}_x^2 + \widetilde{k}_y^2 + \epsilon Q_z^2/\epsilon_\theta$ by the following rescaling and shift of k_y:

$$k_x = \widetilde{k}_x, \quad k_y = \frac{\widetilde{k}_y}{\sqrt{\epsilon_\theta}} - \frac{Q_z(1 - \epsilon)\sin 2\theta}{2\epsilon_\theta}, \quad (A6)$$

where $\epsilon_\theta = \cos^2\theta + \epsilon \sin^2\theta$. Equation (A3) becomes

$$1 = \frac{\sqrt{c_x c_y}}{2\pi h(c_x c_y + 1)\sqrt{\epsilon_\theta}} \int K(\widetilde{R}) \exp\left[-\frac{c_y(\widetilde{k}_x - Q_x)^2}{2h(c_x c_y + 1)}\right.$$
$$\left. - \frac{c_x}{2h(c_x c_y + 1)}\left(\frac{\widetilde{k}_y}{\sqrt{\epsilon_\theta}} - \frac{Q_z(1 - \epsilon)\sin 2\theta}{2\epsilon_\theta} - Q_y\right)^2\right] d^2\widetilde{\mathbf{k}}, \quad (A7)$$

$$\widetilde{R} = \widetilde{k}^2 + \epsilon Q_z^2/\epsilon_\theta. \quad (A8)$$

Here c_x, c_y, and $\mathbf{Q}$ are to be chosen so as to provide the maximum H_{c2}. Since $K(R)$ depends only on $\widetilde{k}^2$, the maximum h corresponds to the lack of linear in $\widetilde{k}_x$ and $\widetilde{k}_y$ terms in the exponent. This yields $Q_x = 0$ and

$$Q_y = -\frac{Q_z(1 - \epsilon)\sin 2\theta}{2\epsilon_\theta} \quad (A9)$$

in agreement with Eq. (10). Then Eq. (A7) takes the form

$$1 = \frac{\sqrt{c_x c_y}}{2\pi h(c_x c_y + 1)\sqrt{\epsilon_\theta}} \int d^2\widetilde{\mathbf{k}} K(\widetilde{R})$$
$$\times \exp\left[-\frac{c_y \widetilde{k}_x^2}{2h(c_x c_y + 1)} - \frac{c_x \widetilde{k}_y^2}{2h\epsilon_\theta(c_x c_y + 1)}\right], \quad (A10)$$

which gives after integration over the polar angle

$$1 = \frac{\sqrt{c_x c_y}}{h(c_x c_y + 1)\sqrt{\epsilon_\theta}} \int_0^\infty d\widetilde{k}\widetilde{k} K(\widetilde{R})$$
$$\times \exp\left[-\frac{\widetilde{k}^2(c_y + c_x/\epsilon_\theta)}{4h(c_x c_y + 1)}\right] I_0\left[\frac{\widetilde{k}^2(c_y - c_x/\epsilon_\theta)}{4h(c_x c_y + 1)}\right], \quad (A11)$$

where $I_0(x)$ is a modified Bessel function. Here h is maximum if the partial derivatives of Eq. (A11) with respect to c_x and c_y vanish. Introducing $c_1 = c_y/(c_x c_y + 1)$ and $c_2 = c_x/(c_c c_y + 1)\epsilon_\theta$, and subtracting the partial derivatives of Eq. (A11) with respect to c_1 and c_2, from each other gives

$$\frac{1}{c_2} - \frac{1}{c_1} = \frac{\sqrt{c_1 c_2}}{h^2} \int_0^\infty K(\widetilde{R})$$
$$\times \exp\left[-\frac{\widetilde{k}^2(c_1 + c_2)}{4h}\right] I_1\left[\frac{\widetilde{k}^2(c_1 - c_2)}{4h}\right] \widetilde{k}^3 d\widetilde{k}. \quad (A12)$$

This equation is satisfied if $c_1 = c_2$, that is, h is maximum if $c_y = c_x/\epsilon_\theta$, and the Bessel function in Eq. (A11) equals unity. Substituting then $c_x = \epsilon_\theta c_y$ into Eq. (A10), shows that the zero derivative with respect to c_y corresponds to the maximum of the function $c_y/(\epsilon_\theta c_y^2 + 1)$. Hence $c_y = \epsilon_\theta^{-1/2}$ and $c_x = \epsilon_\theta^{1/2}$, in agreement with Eq. (8). Equation (A11) then takes the isotropic WHH form

$$1 = \frac{1}{2h_\theta} \int_0^\infty K\left[\widetilde{k}^2 + \frac{\epsilon Q_z^2}{\epsilon_\theta}\right] \exp\left[-\frac{\widetilde{k}^2}{4h_\theta}\right] \widetilde{k} d\widetilde{k} \quad (A13)$$

where $h_\theta = h\sqrt{\epsilon_\theta}$. Dropping tildes and recovering the original units, we reduce Eq. (A13) to Eq. (11).

APPENDIX B: CALCULATION OF U

The summation over n in Eq. (21) is performed inserting $\tan^{-1}(x) = (i/2)\ln[(1 - ix)/(1 + ix)]$ and using $\Sigma_{n=0}^N(n + 1/2)^{-1} = \ln(4\gamma N)$ and $\Sigma_{n=1}^N\ln(n - 1/2 + ia) = \ln[\Gamma(N + 1/2 + ia)/\Gamma(1/2 + ia)]$.[73] Thus

$$\sum_{n=0}^{N}\left[\frac{u}{n+1/2}-\frac{t}{\sqrt{b}}\mathrm{Re}\,\tan^{-1}\frac{u\sqrt{b}}{t(n+1/2)+i\alpha b}\right]=u\,\ln(4\gamma N)$$

$$+\frac{t}{2\sqrt{b}}\mathrm{Im}\,\ln\frac{\Gamma(N_1+ia_1)\Gamma(1/2+ia_2)}{\Gamma(N_1+ia_2)\Gamma(1/2+ia_1)}, \qquad (B1)$$

where $a_1=(\alpha b-u\sqrt{b})/t$, $a_2=(\alpha b+u\sqrt{b})/t$, and $N_1=\Omega/2\pi T_c$ $+1/2\gg 1$. Then Eqs. (B1) and (21) yield

$$U_1=2e^{q^2}\int_q^\infty e^{-u^2}\,\mathrm{Im}\,P(u)du, \qquad (B2)$$

$$P=u\,\ln(4\gamma N)+\frac{t}{2\sqrt{b}}\ln\frac{\Gamma[N_1+ia_1]\Gamma[1/2+ia_2]}{\Gamma[N_1+ia_2]\Gamma[1/2+ia_1]}. \qquad (B3)$$

Equations (B2) and (B3) take into account the effect of the finite ratio $\Omega/2\pi T_c$ on H_{c2}. In the BCS limit, $N\to\infty$, the use of $\ln\Gamma(z)\simeq(z-1/2)\ln z-z$ in Eq. (B3) yields

$$P=u\,\ln(4\gamma)+\frac{t}{2\sqrt{b}}\ln\frac{\Gamma[1/2+i(\alpha b+u\sqrt{b})/t]}{\Gamma[1/2+i(\alpha b-u\sqrt{b})/t]}. \qquad (B4)$$

In the Pauli limit, $\alpha\sqrt{b}\gg 1$, the expansion of the Γ functions in $u\sqrt{b}$ gives after the u integration

$$U_1=\mathrm{Re}\,\psi(1/2+i\alpha b/t)-\psi(1/2), \qquad (B5)$$

where $\psi(z)=d\ln\Gamma/dz$ is the digamma function and $\psi(1/2)$ $=-\ln(4\gamma)$.[73] For $t\to 0$, using again $\Gamma(z)\simeq(z-1/2)\ln z-z$ in Eq. (B4), we calculate the function $D=\ln t+U$, in which $\ln t$ terms cancel out

$$D_1=\ln(4\gamma)-1+\frac{1}{2}\ln b+e^{q^2}\int_q^\infty due^{-u^2},$$

$$[(u+\alpha\sqrt{b})\ln(\alpha\sqrt{b}+u)+[u-\alpha\sqrt{b}]\ln|\alpha\sqrt{b}-u|] \qquad (B6)$$

and $D_2=D_1+\frac{1}{2}\ln\eta$. For $\alpha\sqrt{b}\ll 1$ and $q=0$, Eq. (B6) becomes

$$D_1=\ln(4\gamma)-1+\frac{1}{2}\ln b+2\int_0^\infty e^{-u^2}u\,\ln u\,du=\frac{1}{2}\ln(16\gamma b)-1. \qquad (B7)$$

The paramagnetic terms in Eq. (B6) give corrections $\sim\alpha^2$ $\ll 1$. Substituting Eq. (B7) into Eq. (19) and denoting x $=\ln(16\gamma b/e^2)$ yields the quadratic equation

$$2a_1x+2a_2(x+\ln\eta)+x(x+\ln\eta)=0 \qquad (B8)$$

the solution of which results in Eq. (31).

For $t\to 1$, Eq. (21) can be expanded in $b\ll 1$

$$U_1=2\int_0^\infty\sum_{n=0}^\infty\frac{(u\alpha^2b^2+u^3b/3)}{t^2(n+1/2)^3}e^{-u^2}du=7\zeta(3)(\alpha^2b^2+b/3)/t^2 \qquad (B9)$$

and U_2 is obtained from U_1 by replacing $b\to\eta b$ except the terms, where b is multiplied by α. Then Eq. (19) for H_{c2} in the GL region reduces to

$$a_1(U_1-\tau)+a_2(U_2-\tau)=0 \qquad (B10)$$

the solution of which gives Eq. (28).

[1] Y. Kamihara, T. Watanabe, M. Hirano, and H. Hosono, J. Am. Chem. Soc. **130**, 3296 (2008); K. Ishida, Y. Nakai, and H. Hosono, J. Phys. Soc. Jpn. **78**, 062001 (2009).

[2] I. I. Mazin, D. J. Singh, M. D. Johannes, and M. H. Du, Phys. Rev. Lett. **101**, 057003 (2008); I. I. Mazin and J. Schmalian, Physica C **469**, 614 (2009).

[3] K. Kuroki, S. Onari, R. Arita, H. Usui, Y. Tanaka, H. Kontani, and H. Aoki, Phys. Rev. Lett. **101**, 087004 (2008).

[4] V. Mishra, G. Boyd, S. Graser, T. Maier, P. J. Hirschfeld, and D. J. Scalapino, Phys. Rev. B **79**, 094512 (2009); S. Graser, A. F. Kemper, T. A. Maier, H.-P. Cheng, P. J. Hirschfeld, and D. J. Scalapino, ibid. **81**, 214503 (2010).

[5] W.-Q. Chen, K.-Y. Yang, Y. Zhou, and F.-C. Zhang, Phys. Rev. Lett. **102**, 047006 (2009).

[6] A. Y. Liu, I. I. Mazin, and J. Kortus, Phys. Rev. Lett. **87**, 087005 (2001).

[7] H. J. Choi, D. Roundy, H. Sun, M. L. Cohen, and S. G. Loule, Nature (London) **418**, 758 (2002); Phys. Rev. B **66**, 020513(R) (2002).

[8] A. Floris, G. Profeta, N. N. Lathiotakis, M. Lüders, M. A. L. Marques, C. Franchini, E. K. U. Gross, A. Continenza, and S. Massidda, Phys. Rev. Lett. **94**, 037004 (2005).

[9] F. Hunte, J. Jaroszynski, A. Gurevich, D. C. Larbalestier, R. Jin, A. S. Sefat, M. A. McGuire, B. C. Sales, D. K. Christen, and D. Mandrus, Nature (London) **453**, 903 (2008).

[10] J. Jaroszynski, F. Hunte, L. Balicas, Y.-J. Jo, I. Raičević, A. Gurevich, D. C. Larbalestier, F. F. Balakirev, L. Fang, P. Cheng, Y. Jia, and H.-H. Wen, Phys. Rev. B **78**, 174523 (2008).

[11] A. Yamamoto, L. Balicas, J. Jaroszynski, C. Tarantini, J. Jiang, A. Gurevich, D. C. Larbalestier, R. Jin, A. S. Sefat, M. A. McGuire, B. C. Sales, D. K. Christen, and D. Mandrus. Appl. Phys. Lett. **94**, 062511 (2009).

[12] G. Fuchs, S.-L. Drechsler, N. Kozlova, G. Behr, A. Köhler, J. Werner, K. Nenkov, R. Klingeler, J. Hamann-Borrero, C. Hess, A. Kondrat, M. Grobosch, A. Narduzzo, M. Knupfer, J. Freudenberger, B. Büchner, and L. Schultz, Phys. Rev. Lett. **101**, 237003 (2008); New J. Phys. **11**, 057007 (2009).

[13] S. Khim, J. W. Kim, E. S. Choi, Y. Bang, M. Nohara, H. Takagi, and K. H. Kim, Phys. Rev. B **81**, 184511 (2010).

[14] H. Lei, R. Hu, E. S. Choi, J. B. Warren, and C. Petrović, Phys. Rev. B **81**, 184522 (2010).

[15] M. M. Altarawneh, K. Collar, C. H. Mielke, N. Ni, S. L. Bud'ko, and P. C. Canfield, Phys. Rev. B **78**, 220505 (R) (2008).

[16] M. Kano, Y. Kohama, D. Graf, F. Balakirev, A. S. Sefat, M. A. McGuire, B. C. Sales, D. Mandrus, and S. W. Tozer, J. Phys. Soc. Jpn. **78**, 084719 (2009).

[17] T. Kida, T. Matsunaga, M. Hagiwara, Y. Mizuguchi, Y. Takano, and K. Kindo, J. Phys. Soc. Jpn. **78**, 113701 (2009).

[18] T. Terashima, M. Kimata, H. Satsukawa, A. Harada, K. Hazama, S. Uji, H. Harima, G.-F. Chen, J.-L. Lio, and N.-L. Wang, J. Phys. Soc. Jpn. **78**, 063702 (2009).

[19] M. Fang, J. Yang, F. F. Balakirev, Y. Kohama, J. Singleton, B. Qian, Z. Q. Mao, H. Wang, and H. Q. Yuan, Phys. Rev. B **81**, 020509 (R) (2010).

[20] D. Braithwaite, G. Lapertot, W. Knapo, and I. Sheikin, J. Phys. Soc. Jpn. **79**, 053703 (2010).

[21] G. R. Stewart, Rev. Mod. Phys. **56**, 755 (1984).

[22] Y. Ida, R. Settai, Y. Ota, F. Honda, and Y. Onuki, J. Phys. Soc. Jpn. **77**, 084708 (2008).

[23] Y. Matsuda and H. Shimahara, J. Phys. Soc. Jpn. **76**, 051005 (2007).

[24] J. Singleton and C. Mielke, Contemp. Phys. **43**, 63 (2002).

[25] J. S. Brooks, Rep. Prog. Phys. **71**, 126501 (2008).

[26] A. Gurevich, Phys. Rev. B **67**, 184515 (2003); Physica C **456**, 160 (2007).

[27] A. A. Golubov and A. E. Koshelev, Phys. Rev. B **68**, 104503 (2003).

[28] V. G. Kogan, Phys. Rev. B **66**, 020509 (2002); P. Miranović, K. Machida, and V. G. Kogan, J. Phys. Soc. Jpn. **72**, 221 (2003).

[29] T. Dahm and N. Schopohl, Phys. Rev. Lett. **91**, 017001 (2003).

[30] R. A. Klemm, A. Luther, and M. R. Beasley, Phys. Rev. B **12**, 877 (1975).

[31] S. Takahashi and M. Tachiki, Phys. Rev. B **33**, 4620 (1986); **34**, 3162 (1986).

[32] P. Fulde and R. A. Ferrel, Phys. Rev. **135**, A550 (1964).

[33] A. I. Larkin and Yu. N. Ovchinnikov, Zh. Eksp. Teor. Fiz. **47**, 1136 (1964) [Sov. Phys. JETP **20**, 762 (1965)].

[34] L. W. Grunberg and L. Gunther, Phys. Rev. Lett. **16**, 996 (1966).

[35] E. Helfand and N. R. Werthamer, Phys. Rev. **147**, 288 (1966); N. R. Werthamer, E. Helfand, and P. C. Hohenberg, *ibid.* **147**, 295 (1966).

[36] G. Sarma, J. Phys. Chem. Solids **24**, 1029 (1963); K. Maki, Phys. Rev. **148**, 362 (1966).

[37] A. Bianchi, R. Movshovich, C. Capan, P. G. Pagliuso, and J. L. Sarrao, Phys. Rev. Lett. **91**, 187004 (2003).

[38] M. Radovan, N. A. Fortune, T. P. Murphy, S. T. Hannahs, E. C. Palm, S. W. Tozer, and D. Hall, Nature (London) **425**, 51 (2003).

[39] K. Kumagai, K. Kakuyangi, M. Saitoh, S. Takashima, M. Nohara, H. Takagi, and Y. Matsuda, J. Supercond. Novel Magn. **19**, 1 (2006).

[40] M. Kenzelmann, Th. Sträsle, C. Niedermayer, M. Sigrist, B. Padmanabham, M. Zolliker, A. D. Bianchi, R. Movshovich, E. D. Bauer, J. L. Sarrao, and J. D. Thompson, Science **321**, 1652 (2008).

[41] S. Uji, T. Terashima, M. Nishimura, T. Takahide, T. Konoike, K. Enomoto, H. Cui, H. Kobayashi, A. Kobayashi, H. Tanaka, M. Tokumoto, E. S. Choi, T. Tokumoto, D. Graf, and J. S. Brooks, Phys. Rev. Lett. **97**, 157001 (2006).

[42] R. Lortz, Y. Wang, A. Demuer, P. H. M. Böttger, B. Bergk, G. Zwicknagl, Y. Nakazawa, and J. Wosnitza, Phys. Rev. Lett. **99**, 187002 (2007).

[43] S. Yonezawa, S. Kusaba, Y. Maeno, P. Auban-Senzier, C. Pasquier, K. Bechgaard, and D. Jerome, Phys. Rev. Lett. **100**, 117002 (2008); J. Phys. Soc. Jpn. **77**, 054712 (2008).

[44] M. W. Zwierlein, A. Schirotzek, C. H. Schunk, and W. Ketterle, Science **311**, 492 (2006).

[45] L. Radzihovsky and D. E. Sheehy, Rep. Prog. Phys. **73**, 076501 (2010).

[46] R. Casalbuoni and G. Nardulli, Rev. Mod. Phys. **76**, 263 (2004).

[47] J. P. Brison, N. Keller, V. Vernière, P. Lejay, L. Schmidt, A. Buzdin, J. Flouqet, S. R. Julian, and G. G. Lonzarich, Physica C **250**, 128 (1995).

[48] H. Shimahara, J. Phys. Soc. Jpn. **67**, 1872 (1998).

[49] D. Denisov, A. Buzdin, and H. Shimahara, Phys. Rev. B **79**, 064506 (2009).

[50] L. N. Bulaevskii and A. A. Guseinov, Sov. J. Low Temp. Phys. **2**, 140 (1976).

[51] D. F. Agterberg and K. Yang, J. Phys.: Condens. Matter **13**, 9259 (2001).

[52] I. I. Mazin, M. D. Johannes, L. Boeri, K. Koepernik, and D. J. Singh, Phys. Rev. B **78**, 085104 (2008).

[53] D. J. Singh, Physica C **469**, 418 (2009).

[54] S. Graser, T. A. Maier, D. J. Hirschfeld, and D. J. Scalapino, New J. Phys. **11**, 025016 (2009).

[55] A. I. Coldea, J. D. Fletcher, A. Carrington, J. G. Analytis, A. F. Bangura, J.-H. Chu, A. S. Erickson, I. R. Fisher, N. E. Hussey, and R. D. McDonald, Phys. Rev. Lett. **101**, 216402 (2008).

[56] S. E. Sebastian, J. D. Analytis, J.-H. Chu, I. R. Fisher, and L. Degiorgi, J. Phys.: Condens. Matter **20**, 422203 (2008).

[57] J. G. Analytis, R. D. McDonald, J.-H. Chu, S. C. Riggs, A. F. Bangura, C. Kucharczyk, M. Johannes, and I. R. Fisher, Phys. Rev. B **80**, 064507 (2009).

[58] H. Shishido, A. F. Bangura, A. I. Coldea, S. Tonegawa, K. Hashimoto, S. Kasahara, P. M. C. Rourke, H. Ikeda, T. Terashima, R. Settai, Y. Onuki, D. Vignolles, C. Proust, B. Vignolle, A. McCollam, Y. Matsuda, T. Shibauchi, and A. Carrington, Phys. Rev. Lett. **104**, 057008 (2010).

[59] A. G. Lebed, Phys. Rev. Lett. **96**, 037002 (2006); O. Dutta and A. G. Lebed, Phys. Rev. B **78**, 224504 (2008).

[60] Z. Zheng and D. F. Agterberg, Phys. Rev. B **82**, 024506 (2010).

[61] H. Shimahara, Phys. Rev. B **62**, 3524 (2000).

[62] K. V. Samokhin, Phys. Rev. B **78**, 224520 (2008).

[63] Y. Tada, N. Kawakami, and S. Fujimoto, Phys. Rev. Lett. **101**, 267006 (2008).

[64] C. Mora and R. Combescot, Phys. Rev. B **71**, 214504 (2005).

[65] M. Houzet and V. P. Mineev, Phys. Rev. B **74**, 144522 (2006).

[66] H. Shimahara, Phys. Rev. B **80**, 214512 (2009).

[67] A. I. Buzdin and J. P. Brison, Phys. Lett. A **218**, 359 (1996); Europhys. Lett. **35**, 707 (1996).

[68] L. P. Gor'kov and T. K. Melik-Barkhudarov, Zh. Eksp. Teor. Fiz. **45**, 1493 (1963) [Sov. Phys. JETP **18**, 1031 (1964)].

[69] M. Prohammer and J. P. Carbotte, Phys. Rev. B **42**, 2032 (1990).

[70] M. Schossmann and J. P. Carbotte, Phys. Rev. B **39**, 4210 (1989).

[71] M. Mansor and J. P. Carbotte, Phys. Rev. B **72**, 024538 (2005).

[72] H. Suhl, B. T. Matthias, and L. R. Walker, Phys. Rev. Lett. **3**, 552 (1959); V. A. Moskalenko, Fiz. Met. Metalloved. **8**, 503 (1959) [Phys. Met. Metallogr. **8**, 25 (1959)].

[73] *Handbook of Mathematical Functions*, Applied Mathematics Series Vol. 55, edited by M. Abramowitz and I. R. Stegun (National Bureau of Standards, Washington, D.C., 1964).

[74] L. P. Gor'kov, Zh. Eksp. Teor. Fiz. **37**, 833 (1959) [Sov. Phys. JETP **10**, 539 (1960)].

[75] A. A. Golubov, J. Kortus, O. V. Dolgov, O. Jepsen, Y. Kong, O. K. Anderson, B. J. Gibson, K. Ahn, and R. K. Kremer, J. Phys.: Condens. Matter **14**, 1353 (2002).

[76] L. W. Gruenberg and L. Gunther, Phys. Rev. **176**, 606 (1968).

[77] A. K. Rajagopal and J. C. Ryan, Phys. Rev. B **44**, 10280 (1991).

[78] F. Konschelle, J. Cayssol, and A. I. Buzdin, EPL **79**, 67001 (2007).

[79] B. Bergk, A. Demuer, I. Sheikin, Y. Wang, J. Wosnitza, and R. Lortz, arXiv:1008.3747 (unpublished).

[80] C. Tarantini, M. Putti, A. Gurevich, Y. Shen, R. K. Singh, J. M. Rowell, N. Newman, D. C. Larbalestier, P. Cheng, Y. Jia, and H.-H. Wen, Phys. Rev. Lett. **104**, 087002 (2010).

[81] D. F. Agterberg and H. Tsunestugu, Nat. Phys. **4**, 639 (2008); D. F. Agterberg, Z. Zheng, and S. Mukherjee, Phys. Rev. Lett. **100**, 017001 (2008).

[82] L. Radzihovsky and A. Vishwanath, Phys. Rev. Lett. **103**, 010404 (2009).